Attosecond-resolved electron emission in nonsequential double ionization

Liangyuan Chen,[1] Yueming Zhou,[1,2,*] Cheng Huang,[1] Qingbin Zhang,[1] and Peixiang Lu[1,2,†]

[1]*Wuhan National Laboratory for Optoelectronics and School of Physics, Huazhong University of Science and Technology, Wuhan 430074, China*

[2]*Key Laboratory of Fundamental Physical Quantities Measurement of Ministry of Education, Wuhan 430074, China*

(Received 11 March 2013; published 21 October 2013)

We have investigated the correlated electron dynamics in nonsequential double ionization (NSDI) of xenon by the orthogonally polarized two-color pulses consisting of 800- and 1600-nm laser fields. The two-electron momentum distributions are sensitively dependent on the relative phase of the two pulses. By tracing the history of double ionization trajectories, we find that the revisit time of the returning electron wave packet is controlled with attosecond accuracy. After recollision, one electron is ionized immediately while the other electron is either released immediately or excited with subsequent field ionization. The release time of the excited electron is also steered with attosecond resolution by changing the relative phase of the orthogonal two-color pulses. The attosecond-resolved control of the revisit time of the returning electron wave packet and the release time of the excited electron is responsible for the phase dependence of the correlated behaviors of the two electrons. These results indicate that we can trace the emission of the two electrons in NSDI on attosecond time scales.

DOI: 10.1103/PhysRevA.88.043425 PACS number(s): 32.80.Rm, 31.90.+s, 32.80.Fb

I. INTRODUCTION

Recent advances in femtosecond laser technology have opened the door to unprecedented insight into intense laser-matter interaction, leading to a number of new physical phenomena such as high-order harmonic generation (HHG) [1], above-threshold ionization (ATI) [2], and double ionization (DI) [3]. DI by strong field can proceed through two different ways, sequential double ionization (SDI) and nonsequential double ionization (NSDI). In sequential double ionization, two electrons are ionized near the peak of the electric field one by one almost independently [4,5]. Due to electron-electron interaction, NSDI has attracted utmost attention. In recent years, NSDI has drawn extensive researches experimentally [6] as well as theoretically [7–11]. The differential measurement of recoil ion and emitted electron momenta [12–14] provide a convincing evidence that the NSDI process is governed by the rescattering mechanism [15]. Thereafter, a great number of studies dedicated to the details in the recollision process were performed [16–20].

According to the recolliding mechanism, an electron ionized near the peak of the laser field by tunneling is driven away from its parent ion. When the field reverses its direction, the electron is driven back and recollides with the parent ion which gives rise to the second electron being ionized directly (RCI) or excited with subsequent field ionization (RESI) [13]. Based on this mechanism, steering and identifying the correlated electron dynamics in NSDI can be realized by controlling the recollision process. For example, by changing the phase of the strong few-cycle laser pulse, one can control the returning direction of the recolliding electron, which leads to phase-dependent asymmetric ion momentum distributions in NSDI [21]. Tracing the attosecond electron dynamics is one of the ultimate goals in investigating the correlated electron process in NSDI. Due to its ability to confine the recollisions into a single laser cycle, the few-cycle laser pulse allows one to trace the motions of the electrons and control their dynamics on attosecond time scales. For instance, with phase-stabled few-cycle pulses with a lower intensity, 9×10^{13} W/cm^2, the emission times of the two electrons from the doubly excited state formed by recollision are traced on attosecond time scale [22]. The emission time difference between two electrons is found to be 200 ± 100 as. At a higher intensity, 3×10^{14} W/cm^2, it has been shown that the correlated electron momentum distribution exhibits a cross-shaped pattern [23], which was connected with the RESI process due to the asymmetric energy sharing at recollision [20]. From the correlated electron momentum distribution, the emission of the correlated electrons was traced on subfemtosecond time scales.

It has been demonstrated that the orthogonally polarized two-color laser pulses are an efficient tool to control the spatial and temporal characteristics of the recolliding electron wave packet [24]. For instance, with the orthogonal two-color field (OTC) the recollision angle of the recolliding electron wave packet can be controlled, and thus the molecular orbital symmetry [25] as well as the symmetry of the atomic wave function [26] are successfully probed. Moreover, by controlling the relative phase of the orthogonally polarized two-color pulses, one can steer the revisit time of the recolliding electron wave packet precisely [27]. With this scheme, Brugnera *et al*. demonstrated the control of short and long quantum trajectories in HHG at the single-atom level [28].

For NSDI, the crucial step is also recollision, but the electron dynamics is more complicated. For example, previous studies have shown that the correlated behavior of the electron pairs from NSDI depends on the species of the targets [29,30]. In the single-color field, because of the wide time window of recollision, different pathways of NSDI simultaneously contribute to the final yields in each laser shot, and thus it is difficult to understand the underlying physics of the dependence of the correlated electron behavior on the targets. Carefully steering of the recolliding electron wave packet may help us to understand this complicated electron dynamics more comprehensively. In this paper, we demonstrated that

*zhouymhust@hust.edu.cn
†lupeixiang@mail.hust.edu.cn

via changing the relative phase of the orthogonal two-color fields, the revisit time of the recolliding electron wave packet is controlled with attosecond precision. Because of the precise control on the revisit time of the recolliding electron wave packet, the correlated electron momentum distributions exhibit different correlated behaviors. This indicates that the orthogonal two-color fields can be used to resolve the correlated electron dynamics on attosecond time scale.

II. MODEL

Here, we employ the classical ensemble model [10,11,31–34] to study the correlated electron dynamics in NSDI of xenon by the orthogonal two-color fields. The motions of the two electrons are restricted to the polarization plane of the orthogonal two-color fields because the out-of-plane effects are negligible. The evolution of the two-electron system is governed by Newton's motion equations (atomic units are used throughout this paper unless otherwise stated):

$$\frac{d^2\mathbf{r}_1}{dt^2} = -\frac{2\mathbf{r}_1}{\left(\mathbf{r}_1^2 + a^2\right)^{3/2}} + \frac{\mathbf{r}_1 - \mathbf{r}_2}{[(\mathbf{r}_1 - \mathbf{r}_2)^2 + b^2]^{3/2}} - \mathbf{E}(t), \quad (1)$$

$$\frac{d^2\mathbf{r}_2}{dt^2} = -\frac{2\mathbf{r}_2}{\left(\mathbf{r}_2^2 + a^2\right)^{3/2}} + \frac{\mathbf{r}_2 - \mathbf{r}_1}{[(\mathbf{r}_1 - \mathbf{r}_2)^2 + b^2]^{3/2}} - \mathbf{E}(t), \quad (2)$$

where, $\mathbf{r}_i = x_i\hat{\mathbf{x}} + y_i\hat{\mathbf{y}}$, and the subscript $i = 1,2$ is the label of the two electrons. $\hat{\mathbf{x}}$ and $\hat{\mathbf{y}}$ are the polarization vectors. In order to obtain the initial values, the ensemble is populated in the classically allowed position for the xenon ground-state energy of -1.224 a.u. The remaining kinetic energy is randomly distributed between two electrons in the momentum space. Then the system is allowed to evolve for a sufficiently long time without laser field to obtain stable position and momentum distributions. Note that these distributions in the phase space do not change when we use different methods to obtain the initial state [31]. To avoid autoionization, the screening parameters a and b are set to be 2 and 0.1, respectively. The synthetical electric field is written as $\mathbf{E}(t) = f(t)[E_x(t)\hat{\mathbf{x}} + E_y(t)\hat{\mathbf{y}}]$. $f(t)$ is the laser envelope, which turns on and turns off linearly for two cycles of the 1600-nm field and keeps full strength for six cycles of the 1600-nm field. This envelope facilitates us to study NSDI at a certain laser intensity. $E_x(t) = E_{x0}\cos(\omega t + \phi)$, and $E_y(t) = E_{y0}\cos(2\omega t)$, where E_{x0} is the amplitude of the 1600-nm field. E_{y0} is the amplitude of the 800-nm field. ϕ is the relative phase between the 1600-nm and 800-nm fields. ω is the frequency of the 1600-nm laser field. The intensities of both fields are set to be 5×10^{13} W/cm^2.

Note that the model employed in this paper is completely classical and thus the quantum effects in strong field ionization cannot be captured. However, previous studies have shown that this simple classical model is very successful in exploring the electron dynamics in NSDI [10,32,33]. This is because in NSDI the laser intensity is so strong that the electron motion in the laser field can be well approximated by the motion of a classical particle. More importantly, the critical step of NSDI is the strong electron recollision, which could be well described with a classical method. Providing that the classical treatment is more valid in the long wavelength region, in this paper, the wavelengths of the two-color field are chosen to be 1600 nm + 800 nm though the 800 nm + 400 nm field is more easily accessible in experiment.

III. RESULTS AND DISCUSSIONS

When the intensities of the two fields in the OTC are very different, the weaker field can be treated as a perturbation. In this case, the recollision dynamics is similar to that of the single color field, in the condition that the motion of the electron along the weaker field is offset by a proper initial transverse momentum at tunneling [26]. In our calculations, the intensities of the two pulses are comparable and thus neither of them could be treated as a perturbation. The ionization of the first electron is greatly disturbed as compared to the single-color field. For example, the ionization of the first electron is not along the direction of the 1600-nm field but along the direction of the synthetic field, which could be in any direction of the polarization plane as shown in Fig. 1(a)

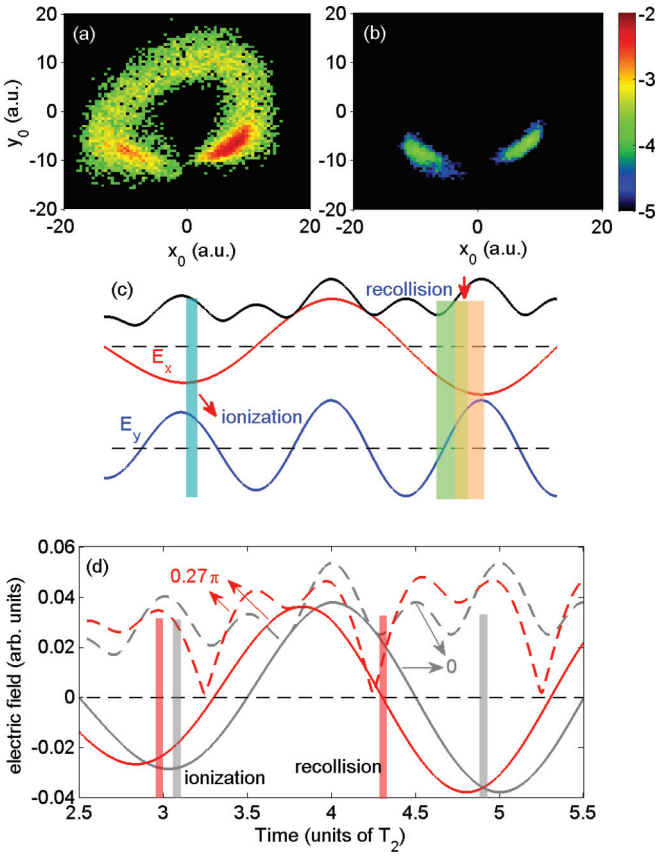

FIG. 1. (Color online) (a) The position distribution of the electrons where all of the trajectories that suffer ionization are included in the orthogonal two-color fields. (b) The same as (a) but only the trajectories that eventually lead to DI are included. The intensities of both pulses are 5×10^{13} W/cm^2. The relative phase $\phi = 0$. (c) Sketch of the roles of two pulses in the orthogonal two-color fields. The brown and green areas represent the time windows for return determined by the fundamental field and by the second-harmonic field, respectively. The black curve represents the amplitude of the synthetical field ($\sqrt{E_x^2 + E_y^2}$). (d) The sketch of the ionization/recollision dynamics for the relative phase $\phi = 0$ and 0.27π, respectively. The dashed curves represent the synthetic electric field. The solid curves denote the electric field of the 1600-nm pulse.

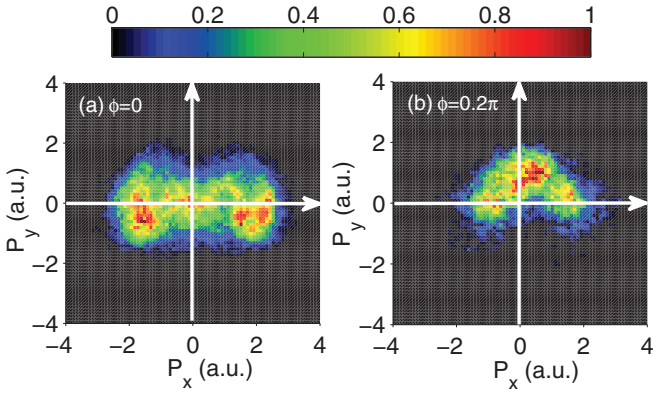

FIG. 2. (Color online) The momentum distributions of Xe^{2+} in the polarization plane for the relative phase $\phi = 0$ and 0.2π, respectively. The distributions are normalized.

[only part of these electrons could be driven back to the parent ion and lead to NSDI, as shown in Fig. 1(b)]. After the first ionization, the evolution of the electron can be considered as two independent motions in the polarization direction of the two fields. In each direction, there is a time window for return. The effective recollision occurs at the overlap region of the two windows, as shown in Fig. 1(c). By changing the relative phase of OTC, the ionization time of the first electron can be manipulated and thus the recollision time windows in both directions change. Consequently, the time window for effective recollision changes, as shown in Fig. 1(d). As shown below, based on this control of the first ionization time and thus the recollision time, the electron dynamics in NSDI can be resolved.

Figure 2 shows the momentum distributions of Xe^{2+} in the polarization plane for the relative phase $\phi = 0$ and 0.2π, respectively. When the relative phase is $\phi = 0$ [Fig. 2(a)], the momentum of Xe^{2+} is clustered around the x axis and shows two peaks in the x direction (the polarization direction of the 1600-nm field). This distribution is very similar to the case of the single-color field [12]. For the relative phase $\phi = 0.2\pi$, the distribution in the x direction is clustered around zero momentum and in the y direction it is located at a positive momentum. The overall dependence of the ion momentum distribution on the relative phase of the two-color field is shown in Fig. 3. Figures 3(a) and 3(b) show the momentum distributions of Xe^{2+} along the polarization direction of the 1600-nm laser field (x axis). The ion momentum distribution in Fig. 3(a) is normalized at each ϕ. The ion momentum spectrum in Fig. 3(b) is normalized with respect to the whole ϕ, which reflects the variation of the DI yields of xenon with the relative phase (as shown in Fig. 4). Figures 3(c) and 3(d) are the same as Figs. 3(a) and 3(b) but for the momentum along the polarization direction of the 800-nm laser field (y axis). As the relative phase changes, the momentum distributions of Xe^{2+} along the x axis and the y axis exhibit a periodical variation. As shown in Fig. 3(a), for $\phi = 0$ the momentum distribution of Xe^{2+} exhibits a double-hump structure. When ϕ increases, the gap in the double-hump structure gradually becomes narrow and finally evolves into a single-hump structure when $\phi = 0.3\pi$. When ϕ further increases from 0.5π to 0.8π, the momentum distribution of Xe^{2+} again evolves from a

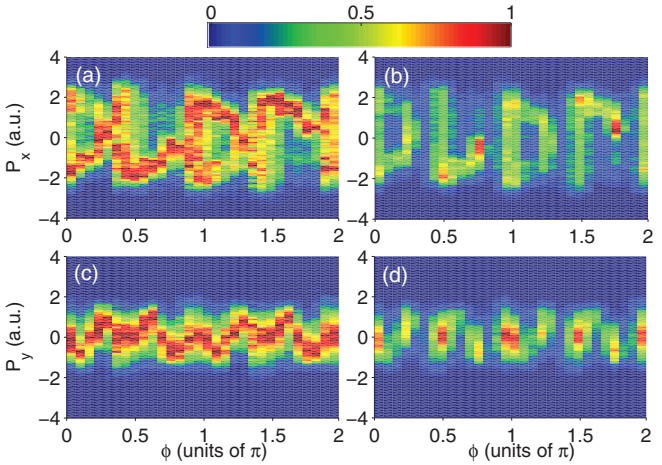

FIG. 3. (Color online) (a) and (b) The momentum distributions of Xe^{2+} along the polarization direction of the 1600-nm laser field as a function of the relative phase ϕ. In (a) the distribution is normalized at each ϕ. In (b) the distribution is normalized with respect to the whole ϕ. (c) and (d) are the same as (a) and (b) but for the momentum along the polarization direction of the 800-nm laser field.

double-hump structure into a single-hump structure. Note that in the long laser pulses the recollision occurs twice every laser cycle of the 1600-nm field and thus the distribution of the ion momentum P_x should be symmetric with respective to $P_x = 0$. However, in Figs. 3(a) and 3(b), one peak (with positive momentum) of the double-hump structure is often much weaker than the other. This unphysical behavior is from the fact that in the classical model a great part of trajectories suffer DI at the turn-on stage of the pulses. In the classical description, the first electron can get ionized more easily at the expense of leaving the second electron near the bottom of the potential well [20,35]. For the soft potential employed in this paper, the potential-energy well for the second electron is about -1 a.u., which is lower than that of realistic xenon. Thus the first electron can be ionized very early at the turn-on stage of the pulse and returns to the parent ion at the turn-on stage, leading to the asymmetric shape in Figs. 3(a) and 3(b). This is also responsible for the asymmetry in the correlated electron momentum distributions shown in Fig. 5. We stress that this unphysical behavior is due to the shortcoming of the simple

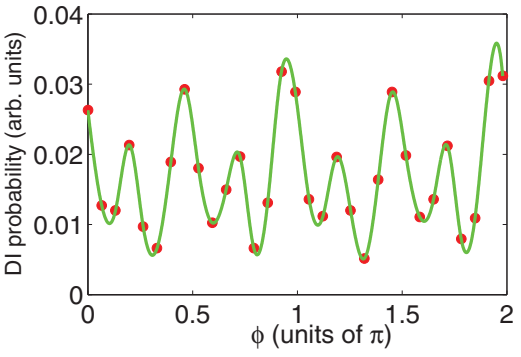

FIG. 4. (Color online) DI yields of Xe as a function of the relative phase ϕ. The green solid curve represents the fitting curve.

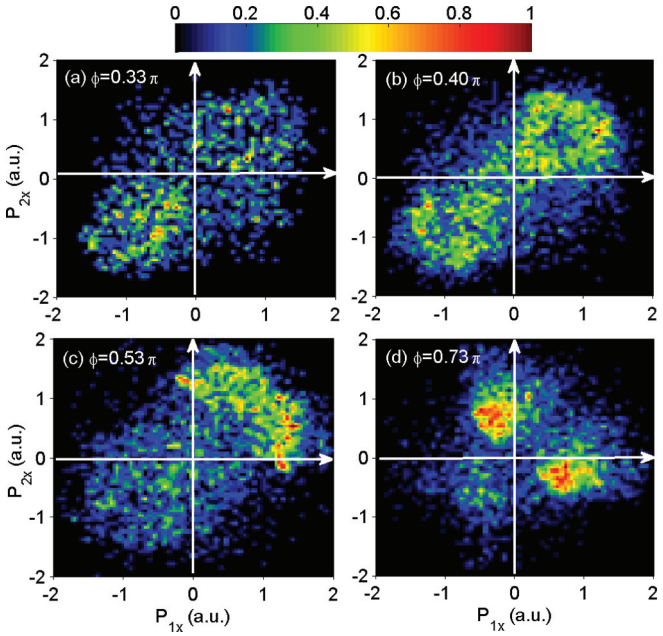

FIG. 5. (Color online) The correlated electron momentum distributions along the polarization direction of the 1600-nm laser pulse for NSDI of xenon by the orthogonal two-color laser pules with the relative phase $\phi = 0.33\pi$, 0.4π, 0.53π, and 0.73π, respectively. The distributions are normalized.

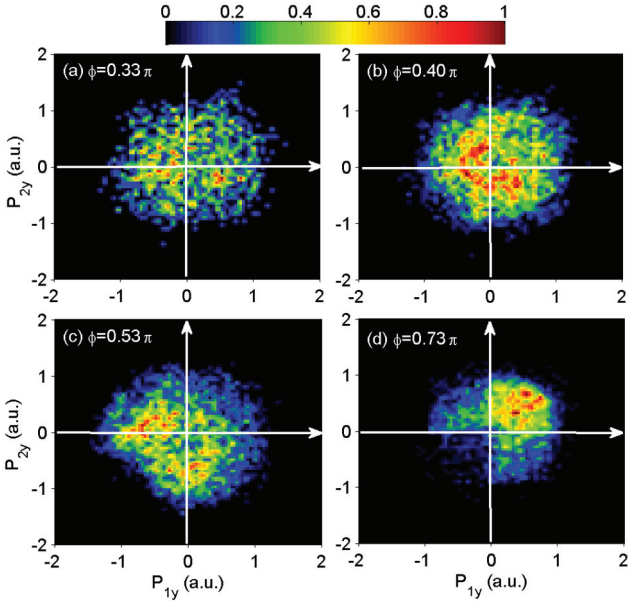

FIG. 6. (Color online) The same as Fig. 5 but for the electron momentum along the polarization direction of the 800-nm laser field. The distributions are normalized.

model. However, this shortcoming does not affect the physics of this paper.

Figure 3(c) shows that the momentum spectrum of Xe^{2+} along the polarization direction of the 800-nm field (y axis) exhibits a single-hump structure, the position of which oscillates near the zero momentum. It is well known that the momentum distribution of Xe^{2+} will exhibit a double-hump structure if the recollision currents repeat every half optical cycle. However, in the orthogonal two-color field the repetition period is one optical cycle of the 800-nm field, not half optical cycle. Thus the momentum distribution of Xe^{2+} along the polarization direction of the 800-nm field exhibits a single-hump structure. In Fig. 4 we display the DI yields of xenon as a function of the relative phase ϕ. When ϕ changes, the DI yields exhibit a periodical variation with a period of 0.5π. It is seen from Fig. 4 that the heights of the peaks in different periods are not the same, which also results from the fact that a considerable part of DI events occur at the turn-on stage of the pulses.

Figure 5 shows the two-electron momentum distributions along the x axis (the polarization direction of the 1600-nm laser pulse), where the relative phases ϕ are 0.33π, 0.40π, 0.53π, and 0.73π, respectively. The correlated electron momentum spectra are symmetric with respect to the diagonal $P_{1x} = P_{2x}$ because the two electrons are not distinguished here. For $\phi = 0.33\pi$, the two-electron momenta are distributed along the diagonal $P_{1x} = P_{2x}$ in the first and third quadrants. When $\phi = 0.4\pi$, the two-electron momenta are distributed in the first and third quadrants and exhibit a repulsive behavior with respect to the diagonal $P_{1x} = P_{2x}$. As ϕ increases to 0.53π, the repulsive behavior becomes more obvious. As ϕ further increases to 0.73π, the correlated electron momentum are distributed in the second and fourth quadrants. These results show that with the increase of the relative phase ϕ the two-electron momentum distribution gradually expands with respect to the diagonal $P_{2x} = P_{1x}$.

In Fig. 6 we display the two-electron momentum spectra along the y axis (the polarization direction of the 800-nm laser pulse). When $\phi = 0.33\pi$, the two-electron momenta are almost uniformly distributed near zero momentum. When $\phi = 0.40\pi$ they mainly clustered in the second and fourth quadrants. For $\phi = 0.53\pi$, the momenta are located around negative values of x and y axes. As ϕ increases to 0.73π, the correlated electron momentum spectrum exhibits an overall maximum in the first quadrant.

The results above reveal that the correlated electron behaviors in NSDI by the orthogonally polarized two-color laser pulses strongly depend on the relative phase. Previous studies have indicated that back analysis of the classical trajectories is an efficient method to explore the responsible dynamical process for the correlated electron behaviors in NSDI [10,17,32]. In order to understand the correlated behavior of the electron pairs in the orthogonal two-color fields, we trace back the history of DI trajectories. Here, we define the recollision time to be the instant of the closest approach of two electrons after the first departure of one electron from the core, and the DI time to be the first time when both electrons gain positive energy, where the energy of an electron contains its kinetic energy, the ion-electron interaction and half electron-electron interaction.

Note that in the single-color laser field, the electron often returns to the parent ion along the polarization direction of the laser field. However, in the orthogonal two-color fields the electron often recollides with the parent ion with different angles at different times [24]. This characteristic has been widely used in probing molecule structure [25]. Figure 7 shows the recollision angle and recollision energy for the relative phase $\phi = 0$ and 0.2π, respectively. It is shown that for $\phi = 0$

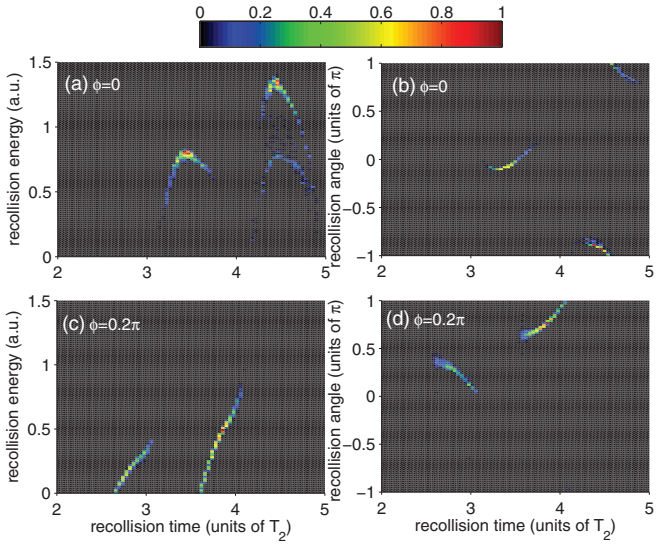

FIG. 7. (Color online) (a) and (b) The recollision energy and the recollision angle of the returning electron wave packet as a function of the recollision time for the relative phase $\phi = 0$. (c) and (d) are the same as (a) and (b) but for the relative phase $\phi = 0.2\pi$. The intensities of two pulses are 5×10^{13} W/cm^2.

there are two groups of recollisions near $4.5T_2$ [see Figs. 7(a) and 7(b)]. These two groups of recollisions correspond to the trajectories that the first electron recollides with the parent ion at its first and second returns (in the polarization direction of the 1600-nm field), respectively. In Fig. 8 we display such two

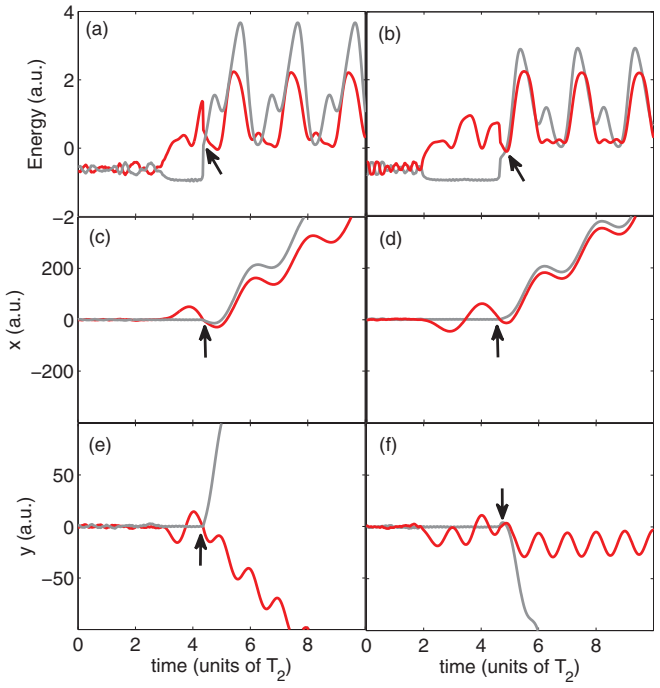

FIG. 8. (Color online) Two sample trajectories for recollision occurring at the first (left column) and second returns (right column) along the x axis, respectively. The upper, middle, and bottom rows show, respectively, the energy, position along the x axis, and position along the y axis versus the time for each electron. The arrows denote the recollision.

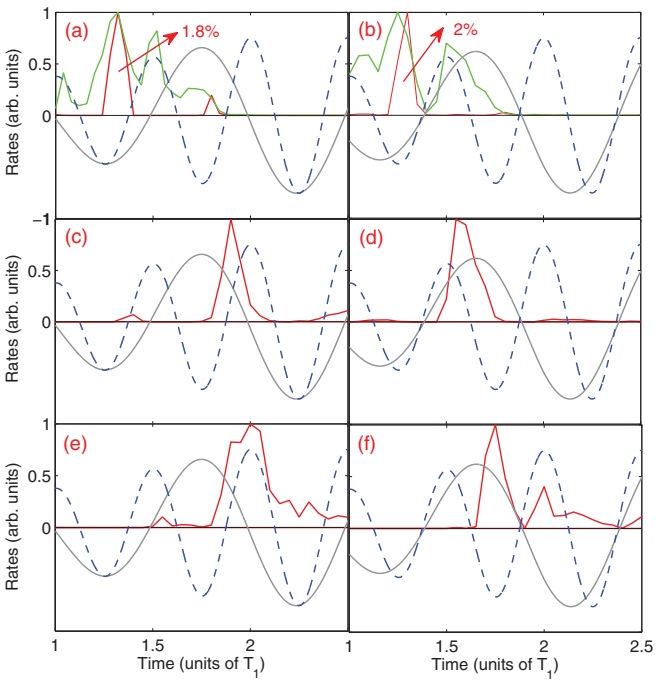

FIG. 9. (Color online) Distributions of the first ionization time (upper row), the recollision time (middle row), and the DI time (bottom row) for DI events for the relative phase $\phi = 0.53\pi$ (left column) and 0.73π (right column), respectively. For (a) and (b), in the green curves all of the trajectories that suffer ionization are included. In the red curves only the trajectories which eventually lead to double ionization are included. The red numbers represent the portion of the first electrons that eventually lead to double ionization. T_1 represents the cycle of the 1600-nm field. The blue dashed and gray solid curves represent the electric fields of the 800-nm and 1600-nm pulses, respectively.

representative trajectories. For the trajectory shown in the left column, the recollision occurs at the first return for the motion along the x axis (the polarization direction of the 1600-nm field) while it corresponds to the second return for the motion along the y axis (the polarization direction of the 800-nm field). For the trajectory shown in the right column, the recollision occurs at the second return for the motion along the x axis and corresponds to the fourth return along the y axis. These two type of trajectories correspond, respectively, to two groups of electrons recolliding with the parent ion around $4.5T_2$ with different angles and energies.

Figure 9 shows the distributions of the first ionization time, the recollision time, and the DI time for DI trajectories where the relative phases are 0.53π (left column) and 0.73π (right column). In the first row of Fig. 9, we also show the ionization time for single ionization trajectories. It shows that only a very small portion of electrons eventually return to the parent ion and lead to NSDI. It is seen from Fig. 9 that the recollision events are clustered in a narrow time window and whereas the DI events are distributed in a wider time window. This is due to the fact that the RESI process also contributes significantly to NSDI besides the RCI process. For the RESI process, one electron possesses positive energy after the recollision process and the other electron is excited by this recollision. The excited electron is often released near the first peak of the

800-nm field after the recollision. For $\phi = 0.53\pi$, as shown in Fig. 9(e), both electrons get ionized near the zero crossing of the 1600-nm field, so the two electrons escape into the same hemisphere along the polarization direction of the 1600-nm laser field [see Fig. 5(c)]. Figure 9(e) also shows that the recollision is around the zero crossing of the 800-nm field and thus the first electron is ionized at this instant. However, the double ionization (the ionization of the second electron) occurs around the peak of the 800-nm field. For this type of DI events, one electron achieves a large final momentum and the other electron achieves almost zero momentum, resulting in the two-electron momentum distribution in Fig. 6(c).

When $\phi = 0.73\pi$, as shown in the right column of Fig. 9, the recollision occurs just before the peak of the 1600-nm field and DI occurs just after the peak of the 1600-nm field. This means that the two electrons are ionized before and after the peak of the 1600-nm field, respectively. Thus two electrons achieve opposite final momentum, resulting in the distribution in the second and fourth quadrants, as shown in Fig. 5(d). As related to the 800-nm field, the recollision is just after the peak of the electric field and DI occurs just before the next peak, and thus both electrons achieve positive final momenta, resulting in the distribution in the first quadrant, as shown in Fig. 6(d). As will be shown below, the recollision time and the electron dynamics of the excited electron change when the relative phase changes, which is responsible for the variation of the correlated patterns in Figs. 5 and 6.

Figure 10 shows the distributions of the travel time from the first ionization to recollision [Fig. 10(a)], the recollision time [Fig. 10(b)], the DI time [Fig. 10(c)], and the delay time between recollision and DI [Fig. 10(d)] as a function of the relative phase ϕ. It is seen from Fig. 10(a) that the travel time changes from about $0.75T_1$ to $0.25T_1$ as the relative phase varies from 0.4π to 0.9π. This indicates that the short or long trajectories are selected by adjusting the relative phase of the two-color field.

Figure 10(b) shows that the first peak in the distribution of the recollision time changes from $3.5T_2$ to $2.5T_2$ and the second peak varies from $4.5T_2$ to $3.5T_2$ when ϕ changes from 0 to 0.4π. When ϕ increases from 0.4π to 0.8π, the recollision time changes from $4T_2$ to $3T_2$. Closer examination of the phase dependence of the recollision time shows that the recollision time changes about 400 attoseconds when the relative phase ϕ increases by 0.05π. This result indicates that the recollision time is controlled with attosecond precision by changing the relative phase of the orthogonal two-color fields.

Figure 10(c) shows that there are two types of trajectories in NSDI by the orthogonal two-color fields. The first one is the RCI process [as shown with a red ellipse in Fig. 10(c)] and the second one is the RESI process [as shown with a white ellipse in Fig. 10(c)]. Figure 10(d) shows the delay time distribution as a function of the relative phase, which more clearly exhibits the features of the two types of trajectories. For the first type of trajectory, the time delay between DI and recollision is clustered at zero. While for the second type of trajectory, the time delay is about $0.25T_2$. As the relative phase increases, the time delay for the second type of trajectory varies gradually and exhibits a periodical variation. These results show that the delay time between recollision and DI in the RESI process is steered accurately by changing the relative phase.

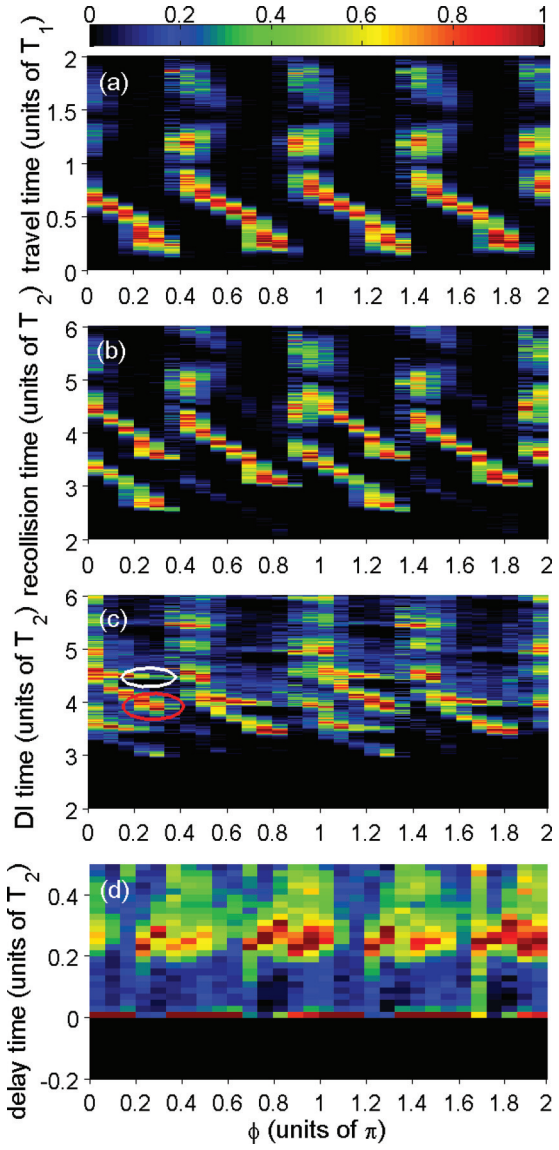

FIG. 10. (Color online) Distributions of the travel time (a), the recollision time (b), the DI time (c), and the delay time (d) as a function of the relative phase. T_2 and T_1 are the laser cycles of the 800- and 1600-nm fields, respectively. The distributions are normalized at each phase.

Further calculations show that the main results above are insensitive to the laser intensity. For example, the behavior of the recollision time, i.e., it moves gradually with the relative phase of the two-color field, does not change with the variation of the laser intensities, as shown in Fig. 11. Nevertheless, some details depend on the laser intensity. For example, when we fix the intensity of the 1600-nm field and decrease the intensity of the 800-nm field, the time window of recollision becomes wider and the movement of the recollision time windows becomes slower, as compared to the case of Fig. 10(b) (see Fig. 11).

The analysis above shows that the revisit time of the recolliding electron wave packet is controlled with attosecond precision. After the recollision, the first electron is ionized immediately and a great number of the second electrons are realeased near the first peak of the 800-nm field, where the

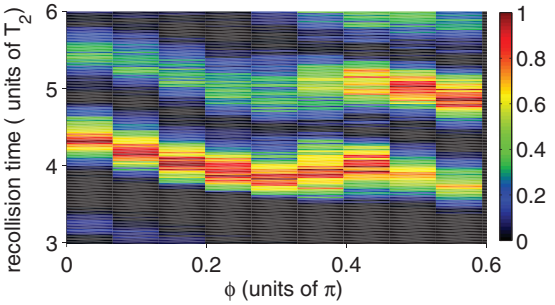

FIG. 11. (Color online) Distribution of the recollision time as a function of the relative phase. The intensities of the 1600-nm laser pulse and the 800-nm laser pulse are 5×10^{13} W/cm^2 and 3.1×10^{12} W/cm^2, respectively. The distribution is normalized at each phase.

delay time between recollision and DI is also steered with attosecond accuracy. This precise control of the revisit time of the recolliding electron wave packet and the delay time between recollision and DI in the RESI process is eventually expressed in the phase-dependent correlated electron behaviors in NSDI. These results mean that the correlated electron dynamics in NSDI at different recollision times are resolved with attosecond accuracy by changing the relative phase of the orthogonal two-color fields.

IV. CONCLUSION

In conclusion, we have investigated the correlated electron dynamics in NSDI of xenon by the orthogonally polarized two-color pulses consisting of an 800- and a 1600-nm laser fields. The results show that the correlated electron behavior depends sensitively on the relative phase of the two-color fields. These phase-dependent correlated behaviors result from the accurate control of the recollision time and the final release time of the electrons by the orthogonal two-color fields. The RESI mechanism is identified with the orthogonal two-color fields and it is clearly displayed in the correlated electron momentum distributions. Different from NSDI by the single-color field where the recollision occurs during a wide time window, in the orthogonal two-color fields, only a selective part of trajectories could return to the parent ion and induce NSDI. Thus, the time window for recollision is much narrower [see in Fig. 9(c)]. This allows one to study the correlated electron dynamics of NSDI more cleanly. Additionally, the position of the narrow time window can be steered precisely and thus enable us to resolve the electron emissions in NSDI with attosecond accuracy. Based on these two advantages, the orthogonal two-color fields might be used to resolve the subtlety of the complex electron dynamics, such as the target dependence of the correlated electron dynamics in NSDI.

ACKNOWLEDGMENTS

This work was supported by the National Natural Science Foundation of China under Grants No. 11004070 and No. 11234004, National Science Fund for Distinguished Young Scholars under Grant No. 60925021, and the 973 Program of China under Grant No. 2011CB808103.

[1] F. Krausz and M. Ivanov, Rev. Mod. Phys. **81**, 163 (2009).
[2] W. Becker *et al.*, Adv. At. Mol. Opt. Phys. **48**, 35 (2002).
[3] A. Becker, R. Dörner, and R. Moshammer, J. Phys. B **38**, S753 (2005); W. Becker, X. Liu, P. J. Ho, and J. H. Eberly, Rev. Mod. Phys. **84**, 1011 (2012).
[4] A. N. Pfeiffer, C. Cirelli, M. Smolarski, R. Döner, and U. Keller, Nat. Phys. **7**, 428 (2011).
[5] Y. Zhou, C. Huang, Q. Liao, and P. Lu, Phys. Rev. Lett. **109**, 053004 (2012); Y. Zhou, Q. Zhang, C. Huang, and P. Lu, Phys. Rev. A **86**, 043427 (2012); Y. Zhou, C. Huang, and P. Lu, Opt. Express **20**, 20201 (2012).
[6] D. N. Fittinghoff, P. R. Bolton, B. Chang, and K. C. Kulander, Phys. Rev. Lett. **69**, 2642 (1992); B. Walker, B. Sheehy, L. F. DiMauro, P. Agostini, K. J. Schafer, and K. C. Kulander, *ibid.* **73**, 1227 (1994); J. B. Watson, A. Sanpera, D. G. Lappas, P. L. Knight, and K. Burnett, *ibid.* **78**, 1884 (1997); C. Guo, M. Li, J. P. Nibarger, and G. N. Gibson, Phys. Rev. A **58**, R4271 (1998); S. Larochelle, A. Talebpoury, and S. L. Chin, J. Phys. B **31**, 1201 (1998); R. Lafon, J. L. Chaloupka, B. Sheehy, P. M. Paul, P. Agostini, K. C. Kulander, and L. F. DiMauro, Phys. Rev. Lett. **86**, 2762 (2001).
[7] A. Becker and F. H. M. Faisal, Phys. Rev. Lett. **84**, 3546 (2000); R. Kopold, W. Becker, H. Rottke, and W. Sandner, *ibid.* **85**, 3781 (2000).
[8] M. Lein, E. K. U. Gross, and V. Engel, Phys. Rev. Lett. **85**, 4707 (2000); Q. Liao, Y. Zhou, C. Huang, and P. Lu, New J. Phys. **14**, 013001 (2012).
[9] J. S. Parker, B. J. S. Doherty, K. T. Taylor, K. D. Schultz, C. I. Blaga, and L. F. DiMauro, Phys. Rev. Lett. **96**, 133001 (2006).
[10] S. L. Haan, L. Breen, A. Karim, and J. H. Eberly, Phys. Rev. Lett. **97**, 103008 (2006); F. Mauger, A. Kamor, C. Chandre, and T. Uzer, *ibid.* **108**, 063001 (2012).
[11] Y. Zhou, Q. Liao, and P. Lu, Opt. Express **18**, 16025 (2010); A. Tong, Q. Liao, Y. Zhou, and P. Lu, *ibid.* **18**, 9064 (2010); C. Huang *et al.*, *ibid.* **19**, 5627 (2011); C. Huang, Y. Zhou, Q. Zhang, and P. Lu, *ibid.* **21**, 11382 (2013).
[12] Th. Weber *et al.*, Nature (London) **405**, 658 (2000); R. Moshammer *et al.*, Phys. Rev. Lett. **84**, 447 (2000).
[13] B. Feuerstein *et al.*, Phys. Rev. Lett. **87**, 043003 (2001).
[14] A. Rudenko, K. Zrost, B. Feuerstein, V. L. B. deJesus, C. D. Schroter, R. Moshammer, and J. Ullrich, Phys. Rev. Lett. **93**, 253001 (2004); E. Eremina *et al.*, J. Phys. B **36**, 3269 (2003).
[15] P. B. Corkum, Phys. Rev. Lett. **71**, 1994 (1993).
[16] Y. Liu, S. Tschuch, A. Rudenko, M. Durr, M. Siegel, U. Morgner, R. Moshammer, and J. Ullrich, Phys. Rev. Lett. **101**, 053001 (2008).
[17] Y. Zhou, Q. Liao, and P. Lu, Phys. Rev. A **80**, 023412 (2009); Y. Zhou, Q. Liao, Q. Zhang, W. Hong, and P. Lu, Opt. Express **18**, 632 (2010).

[18] Q. Liao and P. Lu, Phys. Rev. A **82**, 021403 (2010).
[19] A. Rudenko, V. L. B. de Jesus, T. Ergler, K. Zrost, B. Feuerstein, C. D. Schroter, R. Moshammer, and J. Ullrich, Phys. Rev. Lett. **99**, 263003 (2007); A. Staudte *et al*., *ibid*. **99**, 263002 (2007).
[20] Y. Zhou, Q. Liao, and P. Lu, Phys. Rev. A **82**, 053402 (2010).
[21] X. Liu *et al*., Phys. Rev. Lett. **93**, 263001 (2004).
[22] N. Camus *et al*., Phys. Rev. Lett. **108**, 073003 (2012).
[23] B. Bergues *et al*., Nat. Commun. **3**, 813 (2012).
[24] M. Kitzler and M. Lezius, Phys. Rev. Lett. **95**, 253001 (2005).
[25] H. Niikura, N. Dudovich, D. M. Villeneuve, and P. B. Corkum, Phys. Rev. Lett. **105**, 053003 (2010).
[26] D. Shafir, Y. Mairesse, D. M. Villeneuve, P. B. Corkum, and N. Dudovich, Nat. Phys. **5**, 412 (2009).
[27] Y. Zhou, C. Huang, Q. Liao, W. Hong, and P. Lu, Opt. Lett. **36**, 2758 (2011).
[28] L. Brugnera, D. J. Hoffmann, T. Siegel, F. Frank, A. Zair, J. W. G. Tisch, and J. P. Marangos, Phys. Rev. Lett. **107**, 153902 (2011).
[29] E. Eremina, X. Liu, H. Rottke, W. Sandner, M. G. Schatzel, A. Dreischuh, G. G. Paulus, H. Walther, R. Moshammer, and J. Ullrich, Phys. Rev. Lett. **92**, 173001 (2004).
[30] V. L. B. de Jesus *et al*., J. Phys. B **37**, L161 (2004).
[31] R. Panfili, S. L. Haan, and J. H. Eberly, Phys. Rev. Lett. **89**, 113001 (2002).
[32] P. J. Ho, R. Panfili, S. L. Haan, and J. H. Eberly, Phys. Rev. Lett. **94**, 093002 (2005).
[33] Y. Zhou, C. Huang, and P. Lu, Phys. Rev. A **84**, 023405 (2011); Y. Zhou *et al*., Chin. Phys. Lett. **27**, 123201 (2010).
[34] X. Wang and J. H. Eberly, Phys. Rev. Lett. **103**, 103007 (2009).
[35] S. L. Haan, Z. S. Smith, K. N. Shomsky, and P. W. Plantinga, J. Phys. B **42**, 134009 (2009); Y. Zhou *et al*., Chin. Phys. Lett. **25**, 3950 (2008).